A Modification to the Goldstein Radar Interferogram Filter

Ireneusz Baran, Mike P. Stewart, Bert M. Kampes, Zbigniew Perski, and Peter Lilly

***Abstract*—We present a modification to the adaptive Goldstein radar interferogram filter which improves the quality of interferometry products. The proposed approach makes the Goldstein filter parameter alpha dependent on coherence, such that incoherent areas are filtered more than coherent areas. This modification minimizes loss of signal while still reducing the level of noise.**

***Index Terms*—Phase filtering, phase statistics, radar interferometry, synthetic aperture radar (SAR).**

I. Introduction

ALTHOUGH interferometric synthetic aperture radar (InSAR) applications are well established, the improvement of the interferometry technique and the quality of its products are desirable to further enhance its capabilities. Since the late 80s, many applications of radar interferometry have been developed, including the observation of ground motion over agricultural areas [1], creating high-accuracy digital terrain models (DTMs) [2], and deformation monitoring of the earth's crust with millimeter accuracy at very dense spatial sampling [3]. In addition, InSAR has proven to be a viable method for measuring surface deformation associated with subsidence due to underground mining activities [4].

The application of radar interferometry to DTM production and deformation monitoring encounters problems due to noise in the interferogram phase measurement, which is caused by water vapor in the atmosphere and decorrelation effects that can be categorized as follows: 1) thermal, 2) temporal, 3) geometrical, 4) Doppler centroid, and 5) processing-induced decorrelation [5].

The quality of DTM and displacement maps can be improved by many methods at different processing levels. One of them is filtering of the interferometric phase, as demonstrated in [6]–[10]. However, while filtering reduces noise in the interferogram, it does not necessarily enhance or recover the signal. Furthermore, the impact of the filter can significantly change the structure of the interferogram.

Manuscript received March 18, 2003; revised June 12, 2003. The work of I. Baran was supported by the IPRS Scholarship from Curtin University of Technology, Western Australian School of Mines.

I. Baran and P. Lilly are with The Western Australian School of Mines, Curtin University of Technology, Perth, WA 6845, Australia (e-mail: I.Baran@curtin.edu.au; lillyp@wasm.curtin.edu.au).

M. P. Stewart is with The Western Australian Centre for Geodesy, Curtin University of Technology, Perth, WA 6845, Australia (e-mail: stewart@vesta.curtin.edu.au).

B. M. Kampes is with the German Aerospace Center (DLR), Oberpfaffenhofen 82234, Germany (e-mail: Bert.Kampes@dlr.de).

Z. Perski is with the Department of Geological Mapping, University of Silesia, Sosnowiec 41-200, Poland (e-mail: Perski@us.edu.pl).

Digital Object Identifier 10.1109/TGRS.2003.817212

II. Goldstein Radar Interferogram Filter

Goldstein and Werner [9], [10] proposed an adaptive radar interferogram filter based on the concept of multiplication of the Fourier spectrum $Z(u,v)$ of a small interferogram patch by its smoothed absolute value $S\{|Z(u,v)|\}$ to the power of an exponent α

$$H(u,v) = S\{|Z(u,v)|\}^{\alpha} \cdot Z(u,v) \tag{1}$$

where $H(u,v)$ is the filter response (the spectrum of the filtered interferogram); $S\{\}$ is a smoothing operator; u and v are spatial frequencies; and α is the filter parameter. Patches are defined as a small part of the interferogram and are overlapped to prevent discontinuities at the boundaries. The filter parameter α is an arbitrarily chosen value between zero and one and has the biggest impact on the filter performance. For the value of $\alpha = 0$, the multiplication factor becomes one, and no filtering occurs. However, for large values of α, the filtering is significant.

A problem using the Goldstein radar interferogram filter occurs when a high value of the parameter α is applied. By subtracting the filtered from the unfiltered interferogram, a residual systematic phase trend appears, indicating a loss of resolution in the filtered phase [10].

III. Filter Modification

The quality of the interferometric phase can be estimated directly from the interferometric data as a function of the complex coherence (γ) between two complex SAR images g_M and g_S (the interferometric pair) [11]

$$\gamma = \frac{E\{g_M g_S^*\}}{\sqrt{E\left\{|g_M|^2\right\} E\left\{|g_S|^2\right\}}} \tag{2}$$

or derived theoretically based on the sensor characteristics, signal processing algorithms, and acquisition conditions.

Bamler and Hartl [12] define the phase standard deviation for a single-look ($L = 1$) interferogram as a function of the absolute value of the complex coherence $|\gamma|$ given by

$$\sigma^2_{\varphi,L} = \frac{\pi^2}{3} - \pi \arcsin(|\gamma|) + \arcsin^2(|\gamma|) - \frac{Li_2\left(|\gamma|^2\right)}{2} \tag{3}$$

where Li_2 is the Euler's dilogarithm, defined as

$$Li_2\left(|\gamma|^2\right) = \sum_{k=1}^{\infty} \frac{|\gamma|^{2k}}{k^2}. \tag{4}$$

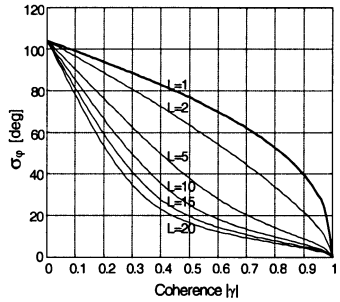

Fig. 1. Phase standard deviation (σ_φ) versus absolute coherence (L indicates the multilook number).

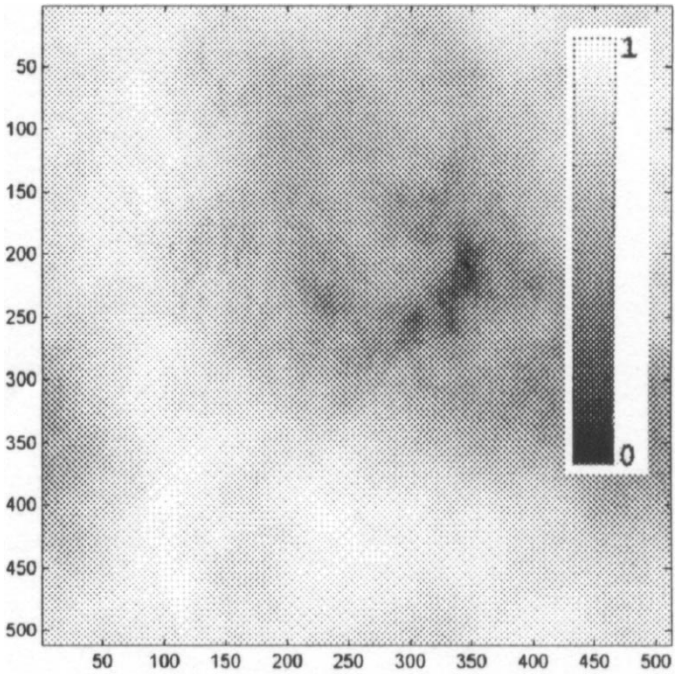

Fig. 2. Simulated coherence map (multilook factor $L = 1$).

Fig. 1 shows the relationship between the absolute coherence $|\gamma|$ and phase standard deviation σ_φ. It shows that the phase standard deviation is reduced as either the number of looks or coherence increases. From the relationship expressed in (3), the coherence can be recognized as a direct measure of the interferogram phase noise. Therefore, it can be used to modify the Goldstein interferogram filter. The filter is modified by making the parameter α in (1) dependent on the value of absolute coherence

$$H(u,v) = S\{|Z(u,v)|\}^{1-\overline{\gamma}} \cdot Z(u,v). \tag{5}$$

Equation (5) shows the modified Goldstein radar interferogram filter, where the exponent α has been replaced by $1-\overline{\gamma}$. The parameter $\overline{\gamma}$ is the mean value of the absolute coherence computed over the effective corresponding patch (patch minus overlap) on the coherence map. This approach insures that the coherence and filter response are of the same size and in the same place. Furthermore, it prevents $\overline{\gamma}$ being affected by the coherence from the overlapped part of the patch.

TABLE I
FILTER PARAMETERS

Filter type	Patch size	Overlap	Smoothing operator S{}	Filter parameter
Goldstein	32x32	14	mean kernel (3x3)	$\alpha = 0.9$
Modified Goldstein	32x32	14	mean kernel (3x3)	$1-\overline{\gamma}$

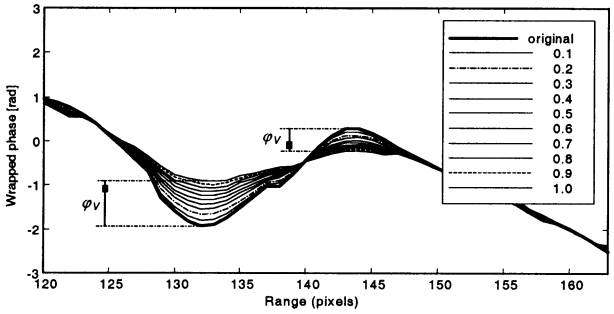

Fig. 3. Cross section over the simulated interferogram without noise. Each line shows the phase after filtering for different value of the filter exponent. The phase offsets (φ_V) are clearly visible.

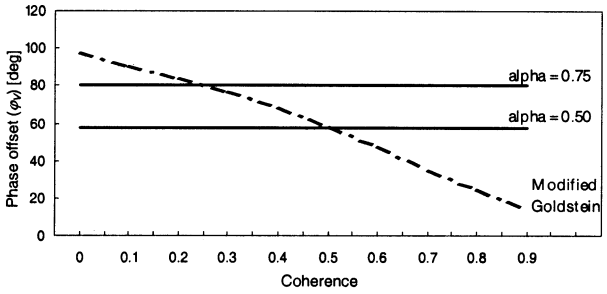

Fig. 4. Mean absolute coherence versus $\pm\max$ phase offset caused by the Goldstein (horizontal lines) and modified Goldstein filter (dashed line).

The new filter parameter is automatically set up based on the coherence value and without any user input. Such a modification adapts the Goldstein interferogram filter by preventing the areas of high coherence (less noise) being overfiltered, but allows stronger filtering in areas where there is a low coherence (high noise). Thus, the loss of resolution in the interferogram due to filtering can be reduced in the areas where the coherence is high.

The interferogram and the coherence map are divided into overlapping rectangular patches. Patches are defined as a small part of the interferogram of even-sized pixels (power of two), which ensures fast Fourier transform (FFT) efficiency. The overlap between patches is required to prevent discontinuities at the boundaries. The maximum overlap size is described as the half of the patch size minus one. The choice of overlap size of 14 pixels in the subsequent section and Table I represents a tradeoff between computation time and minimization boundary effects.

For each patch of the interferogram, the spectrum $Z(u,v)$ is computed (using two-dimensional FFT). At the same time, from the effective corresponding patch on the coherence map the mean value $\overline{\gamma}$ is computed. Finally, the spectrum of the interferogram patch is weighted by multiplying it by its smoothed

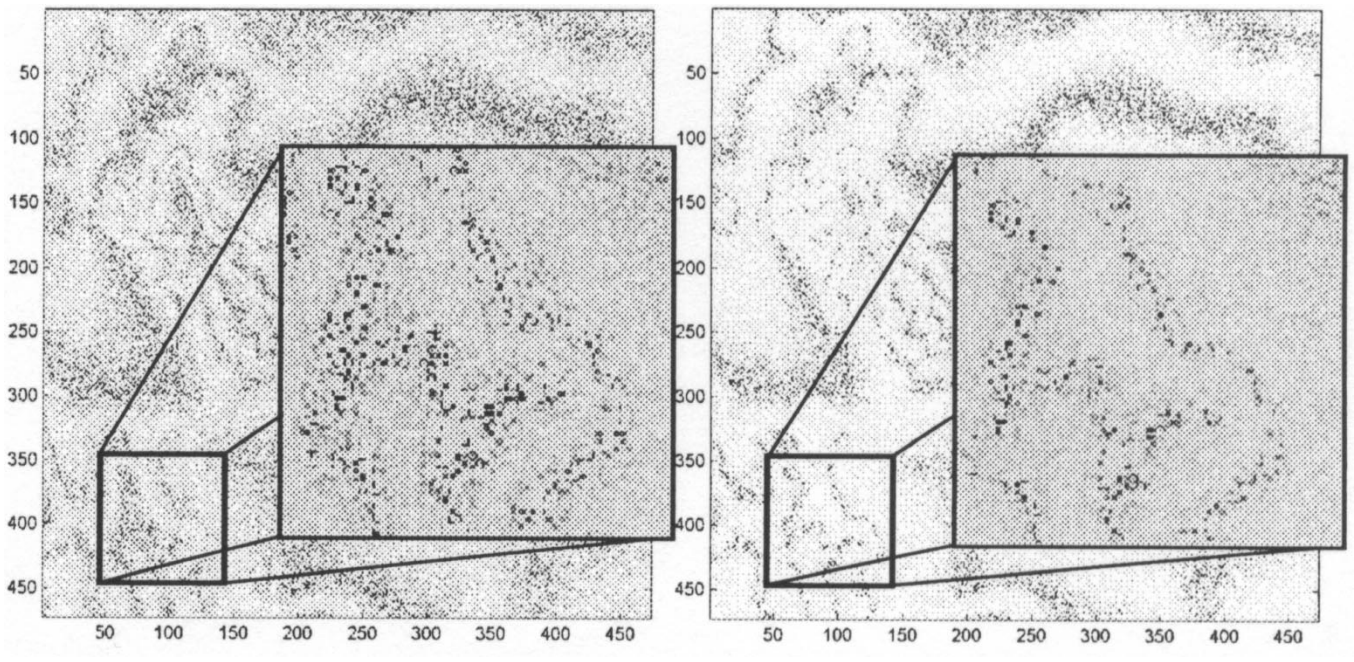

Fig. 5. (a) Differences between filtered and unfiltered simulated interferogram for Goldstein and (b) for modified Goldstein filter.

and scaled absolute spectrum to the power of an exponent $1-\overline{\gamma}$. Smoothing of the absolute spectrum is performed by spatial convolution with a block kernel ($S\{\}$). As the block kernel, the Fourier spectrum of the spatial moving average has been applied. The size of the smoothing kernel must be small to prevent the spectrum being oversmoothed.

IV. Numerical Validation Using a Simulated Dataset

The performance of the filter modification was analyzed using simulated and real interferometry data. The wrapped phase interferogram was simulated by radar-coding a given DTM and wrapping its phase. Although the Goldstein filter uses amplitude (the complex signal is filtered), the amplitude was not simulated, as it is not required for reliable results. The coherence map was simulated based on three decorrelation effects [5]: 1) geometrical (based on DTM), 2) thermal (based on European Remote Sensing 1 and 2 (ERS-1/2) satellite sensor specifications), and 3) temporal (fractal surface), so the final coherence was estimated as the product of each of the decorrelation factors (Fig. 2). Based on the relationship that links phase variance (σ_φ^2) with the absolute value of the complex coherence (3), a matrix of standard deviations was generated from the modeled coherence map.

A Gaussian noise matrix was computed by pointwise multiplication of the phase standard deviation matrix with a matrix of normally distributed random numbers with mean zero and variance one. Finally, the noise was added to the simulated interferogram.

To this simulated dataset the Goldstein and modified Goldstein interferogram filters were applied and tested. The filter parameters for all tests are listed in Table I. The idea of choosing the filter parameter $\alpha = 0.9$ was that this value demonstrates relatively large impact on the filter performance and the loss of the signal.

TABLE II
Used Datasets of Radar Images

Product / Satellite	Orbit	Frame	Acquisition date
SLC / ERS-1	22650	4164	14-Nov-1995
SLC / ERS-2	9991	4164	19-Mar-1997

In the first test, the modified Goldstein interferogram filter was used to filter the interferogram without any noise at all to assess the filter impact on the wrapped phase itself in terms of the filter parameter $1-\overline{\gamma}$. The uniform coherence value is assumed to be over the entire interferogram each time filtering is applied. Filtering was performed for coherences from 0.0 up to 0.9 with a step of 0.1. Fig. 3 shows an example cross section over the simulated interferogram without noise, which shows the sample of a number of cross sections analyzed. Vertical offsets (φ_V) between the original and filtered phase due to impact of the filter can be seen. The magnitude of the offset increases as the filter parameter $1-\overline{\gamma}$ increases. Furthermore, the biggest vertical offsets are experienced in areas of large curvature and they always occur in the direction of concavity.

Fig. 4 shows the characteristics of the Goldstein and modified Goldstein interferogram filter in terms of the $\pm\max$ phase offset caused by the filters, versus the mean absolute coherence ($\overline{\gamma}$). The graph is constructed based on the phase differences between the interferogram without noise and its filtered versions. The dashed line on the graph shows the $\pm\max$ phase offsets for the modified Goldstein filter. It appears that for high coherence values, the phase offsets become small. After analyzing the whole interferogram, the maximum differences between the original and filtered phase were found to be $\pm 98^\circ$ for $\overline{\gamma}=0$ and $\pm 14^\circ$ for $\overline{\gamma}=0.9$. On the other hand, the two horizontal lines

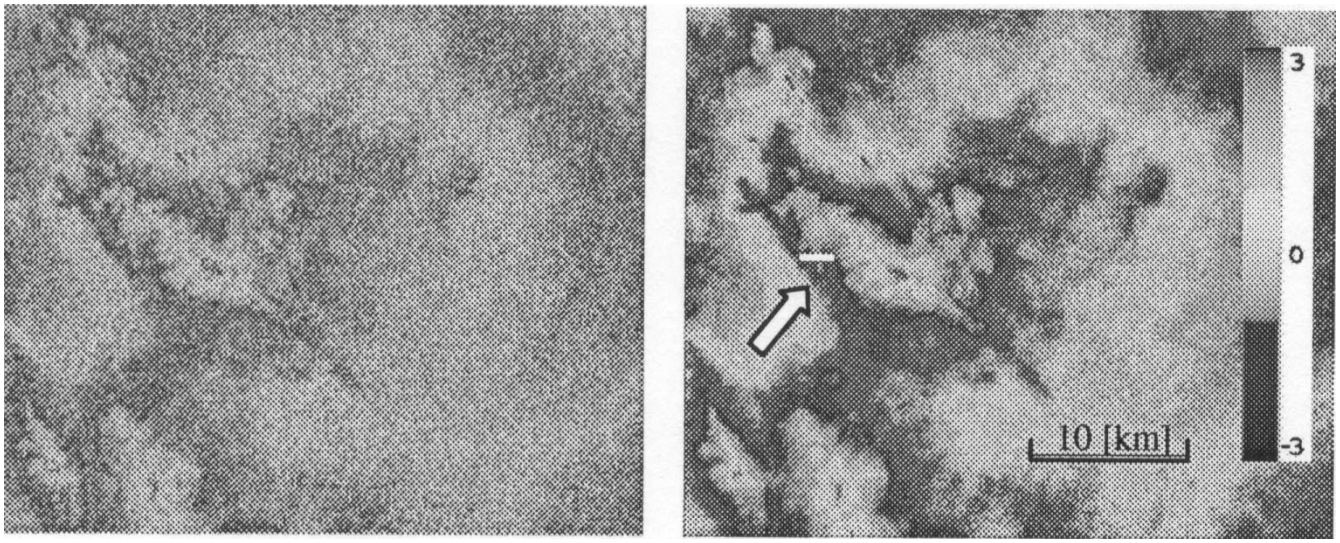

(a) (b)

Fig. 6. (a) Unfiltered and (b) filtered wrapped phase interferogram using modified Goldstein interferogram filter. The arrow indicates cross-section location (color bar in radians).

show the expected $\pm \max$ phase offset for the Goldstein filter and two different values of parameter α : $\pm 80^{\circ}$ for $\alpha = 0.75$ and $\pm 59^{\circ}$ for $\alpha = 0.50$.

In this case, the differences between the original and filtered phase are high, constant and strongly dependent on the chosen α value.

In the next test, both filters were applied to the simulated phase interferogram with noise and the simulated coherence map. The differences between the filtered interferogram and its original version were determined and are shown in Fig. 5. The visible patterns show the systematic phase trend indicating some loss of resolution in the filtered interferogram. Both filters lead to some loss of resolution. However, the modified filter reduces loss of resolution over the part of the interferogram that is characterized by higher coherence. The rectangular windows in Fig. 5 show the area where the major differences between the filters occur.

V. Numerical Validation Using a Real Dataset

In the final test both filters were applied to real data. Two radar images acquired by satellites ERS-1 and ERS-2 over the Western Australia Goldfields mining region have been processed using the Delft University public domain InSAR software "Doris" [13]. The perpendicular baseline is 195 m. The radar image details are listed in Table II. The precise orbits for the satellites provided by Delft were used [14].

After filtering the interferogram, an improvement in the phase noise is clearly visible (Fig. 6). A closer look at the example cross section (Fig. 7) over the wrapped phase interferogram shows the same characteristics of the Goldstein filter and its modified version observed in the simulated dataset. The horizontal line on Fig. 6(b) indicates the cross-section location. On Fig. 7, the circle "A," large vertical phase offset φ_V can be observed for the Goldstein filter. At the same time, due to the high coherence ($\overline{\gamma} > 0.7$) in this region, the modified Goldstein filter does not create the high phase offset.

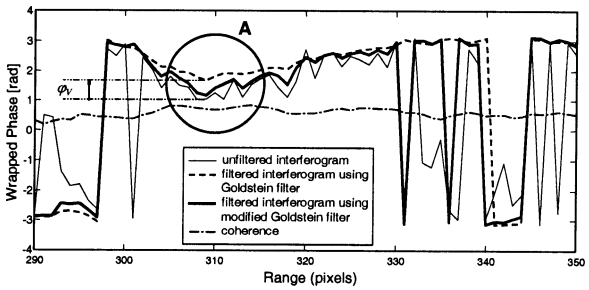

Fig. 7. Cross section over the unfiltered and filtered wrapped phase interferogram.

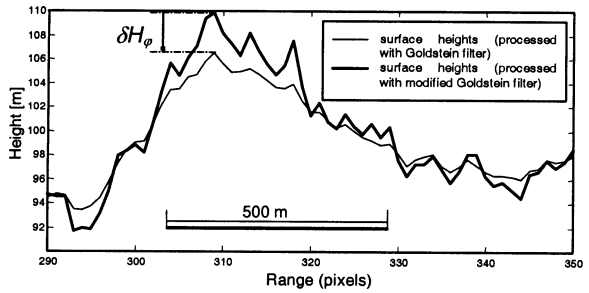

Fig. 8. Cross section over the surface heights.

To check how the phase offset affects terrain heights, phase unwrapping and height computation were performed using SNAPHU, phase unwrapping software developed by the Interferometry Group at Stanford University. SNAPHU implements the Statistical-cost, Network-flow algorithm for phase unwrapping proposed by Chen and Zebker [15]. Fig. 8 shows the cross section over the surface heights along the same location as Fig. 7.

As expected, the vertical phase offset propagates directly into the height of the DTM introducing additional systematic error ($\delta H \varphi$). The magnitude of such error depends strongly on φ_V and is proportional to the height ambiguity. In the same way the phase offset will propagate into the deformation map leading to

some loss of resolution. The improvement of the modified filter when applied to deformation monitoring may also be significant if the deformation signal is very small.

VI. Conclusion

Modification to the Goldstein interferogram filter has been proposed. The filter parameter α is replaced by the new parameter $1-\overline{\gamma}$ that is dependent on the value of absolute coherence. This modification adapts the filter to the wrapped phase interferogram more effectively by preventing the areas characterized by high coherence being overfiltered. On the other hand, it allows stronger filtering on the areas with low coherence. However, both filters perform almost identically in the areas where coherence is low (less than 0.3).

In summary, interferograms that are characterized by high coherence will benefit from the modified Goldstein radar interferogram filter, as it decreases loss of resolution. In particular, interferograms of regions of rough terrain should benefit when the modified Goldstein filter is used.

Acknowledgment

The European Space Agency (ESA) supplied SAR data under Project 1123. The authors would like to thank the four anonymons reviewers who provided valuable and constructive comments on the earlier version of this letter.

References

[1] A. K. Gabriel, R. M. Goldstein, and H. A. Zebker, "Mapping small elevation changes over large areas: Differential radar interferometry," *J. Geophys. Res.*, vol. 94, no. B7, pp. 9183–9191, 1989.

[2] H. A. Zebker and R. M. Goldstein, "Topographic mapping from interferometric synthetic aperture radar observations," *J. Geophys. Res.*, vol. 91, no. B5, pp. 4993–4999, 1986.

[3] T. Strozzi, U. Wegmüller, Ch. Werner, and A. Wiesmann, "Measurement of slow uniform surface displacement with mm/year accuracy," in *Proc. IGARSS*, July 2000, pp. 2239–2241.

[4] Z. Perski, "The test of applicability of land subsidence monitoring by InSAR ERS-1 and ERS-2 in the coal mine damaged region (Upper Silesia)," *Int. Arch. Photogramm. Remote Sens.*, vol. 32, no. 7, pp. 555–558, 1998.

[5] H. A. Zebker and J. Villasenor, "Decorrelation in interferometric radar echoes," *IEEE Trans. Geosci. Remote Sensing*, vol. 30, pp. 950–959, Sept. 1992.

[6] B. Reeves, J. Homer, G. Stickley, D. Noon, and I. D. Longstaff, "Spatial vector filtering to reduce noise in interferometric phase images," in *Proc. IGARSS*, Hamburg, Germany, June 1999, pp. 260–263.

[7] G. Bo, S. Dellepiane, and G. Beneventano, "A locally adaptive approach for interferometric phase noise reduction," in *Proc. IGARSS*, Hamburg, Germany, 1999, pp. 264–266.

[8] J.-S. Lee, P. Papathanassiou, T. L. Ainsworth, R. Grunes, and A. Reigber, "A new technique for noise filtering of SAR interferometric phase images," *IEEE Trans. Geosci. Remote Sensing*, vol. 36, pp. 1456–1464, Sept. 1998.

[9] R. M. Goldstein and C. L. Werner, "Radar ice motion interferometry," in *Proc. 3rd ERS Symp.*, vol. 2, Florence, Italy, 1997, pp. 969–972.

[10] ——, "Radar interferogram filtering for geophysical applications," *Geophys. Res. Lett.*, vol. 25, no. 21, pp. 4035–4038, 1998.

[11] R. Bamler and D. Just, "Phase statistics and decorrelation in SAR interferometry," in *Proc. IGARSS*, 1993, pp. 980–984.

[12] R. Bamler and P. Hartl, "Synthetic aperture radar interferometry," *Inv. Prob.*, vol. 14, pp. R1–R54, 1998.

[13] B. Kampes and S. Usai, "Doris: The Delft object-oriented radar interferometric software," in *Proc. 2nd Int. Symp. Operationalization of Remote Sensing*, Enschede, The Netherlands, Aug. 16–20, 1999.

[14] R. Scharroo and P. Visser, "Precise orbit determination and gravity field improvement for the ERS satellites," *J. Geophys. Res.*, vol. 103, no. C4, pp. 8113–8127, 1998.

[15] C. W. Chen and H. A. Zebker, "Two-dimensional phase unwrapping with use of statistical models for cost functions in nonlinear optimization," *J. Opt. Soc. Amer. A*, vol. 18, pp. 338–351, 2001.